2018 IEEE Conference on Decision and Control (CDC)
Miami Beach, FL, USA, Dec. 17-19, 2018

Adaptive Squaring-Based Control Allocation for Wide Systems with Application to Lateral Flight Control

Ankit Goel, Ahmad Ansari, and Dennis S Bernstein

Abstract— **Redundant actuators provide the opportunity to allocate control effort to account for saturation and other input constraints. This is especially true in wide systems, where the number of input channels is greater than the number of outputs. The present paper considers the control allocation problem within the context of adaptive control. In particular, for retrospective cost adaptive control (RCAC), the target model is shown to constrain the direction of the vector of inputs. This directional constraint is used within RCAC to enforce control allocation across the input channels of wide systems. This approach is applied to the allocation of rudder and aileron inputs for lateral flight control.**

I. Introduction

Many control applications possess the mixed blessing of more actuators than controlled outputs. For these applications, the required control inputs can be realized by combinations of redundant actuators, thus providing reliability. At the same time, however, the presence of actuators with similar effect on the system demands that these actuators be used optimally with respect to magnitude and rate saturation, energy usage, and other limitations. This is the *control allocation problem* [1], [2].

Control allocation is widely studied within the context of aerospace vehicles [3]–[6], where the moments obtainable from control surfaces are limited by there size and depend on the current the aircraft speed. A classical case of actuator redundancy in lateral flight control concerns the use of ailerons and rudders to perform turning maneuvers. Separate use of these actuators for turning yields poor performance, however, due to adverse aileron yaw and adverse rudder roll. Consequently, control allocation can ensure that the ailerons and rudder are used in a desirable combination to perform coordinated turns.

In the present paper, we consider control allocation within the context of retrospective cost adaptive control (RCAC) [7]. RCAC is a direct digital control technique that is applicable to stabilization, command following, and disturbance rejection. A key feature of RCAC discussed in [7] is the role of the filter $G_{\rm f}$ in defining the retrospective cost variable. As shown in [7], $G_{\rm f}$ serves as a target model for the intercalated transfer function from the virtual external control perturbation to the performance variable. Modeling information concerning the leading numerator sign, relative degree, and nonminimum-phase (NMP) zeros is used to construct $G_{\rm f}$.

The present paper extends the development of [7] by focusing on wide (that is, overactuated) systems for the purpose of control allocation. In particular, we show that the applied control input lies in the range of the target model. For example, if the plant is MISO and the target model $G_{\rm f}$ is chosen to be $G_{\rm f}(\mathbf{q}) = N_1\frac{1}{\mathbf{q}}$, where $\mathbf{q}$ is the forward shift operator and N_1 is a row vector, then the control input vector is constrained to the direction $N_1^{\rm T}$. For example, if the plant has two inputs and one output and N_1 is chosen to be $N_1 = [3\ \ 6]$, then, for all time steps k, $u_1(k)/u_2(k) = 1/2$. Consequently, the target model provides a simple and convenient technique for control allocation in overactuated systems.

The contents of the paper are as follows. Section II states the control allocation problem. Next, Section III reviews RCAC, and Theorem III.1 demonstrates how the target model constrains the allowable directions of the control input. Section IV presents several examples illustrating control allocation for RCAC. Section V applies RCAC to lateral control of the NASA GTM model, while constraining the ratio of aileron and rudder control inputs for lateral turn control. The paper ends with some conclusions and directions for future research.

II. Control allocation problem

Consider the MIMO discrete-time plant

$$x(k+1) = Ax(k) + Bu(k) + D_1 w(k), \tag{1}$$

$$y(k) = Cx(k) + D_2 w(k), \tag{2}$$

$$z(k) = Ex(k) + E_2 w(k), \tag{3}$$

where $x(k) \in \mathbb{R}^{l_x}$ is the state, $y(k) \in \mathbb{R}^{l_y}$ is the measurement, $u(k) \in \mathbb{R}^{l_u}$ is the control signal, $w(k) \in \mathbb{R}^{l_w}$ is the exogenous signal, and $z(k) \in \mathbb{R}^{l_z}$ is the performance variable. The components of w can represent either command signals to be followed, external disturbances to be rejected, or both. Figure 1 shows a block diagram representation of (1)–3.

The goal is to develop an adaptive output-feedback controller that produces the control effort in a desired ratio and minimizes z in the presence of the exogenous signal w with limited modeling information about (1)–3 .

In this paper, we consider overactuated systems, that is, $l_u > l_y$. In overactuated systems, the control input required to generate a desired output is not unique. For example, consider step command following for a two-input, one-output LTI plant. At steady state,

$$y_\infty = C(I-A)^{-1}Bu_\infty, \tag{4}$$

where $y_\infty \in \mathbb{R}$ is the asymptotic output of the plant, and $u_\infty \in \mathbb{R}^2$ is the asymptotic control input. Since $C(I-A)^{-1}B$ is a

The authors are with the Department of Aerospace Engineering, University of Michigan, Ann Arbor, MI 48109.

wide matrix, it follows that the asymptotic control input u_∞ is not unique. The goal of the control allocation problem is thus to achieve the specified performance objectives while confining the control input vector u to a chosen subspace that constrains the direction of the allowable control inputs.

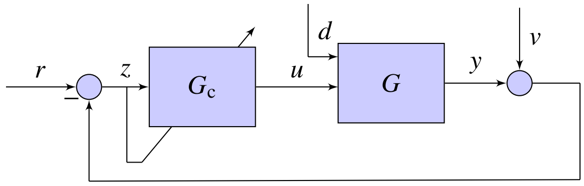

Fig. 1: Block diagram representation of the adaptive control allocation problem with the adaptive controller G_c and plant G. The goal is to design the controller G_c that produces the control effort in a desired ratio such that the plant output y follows the reference command r in presence of process noise d and measurement noise v.

III. RCAC ALGORITHM

We consider a dynamic compensator represented by an ARMA model with a built-in integrator. The control $u(k)$ is thus given by

$$u(k)=\sum_{i=1}^{n_c}P_i(k)u(k-i)+\sum_{i=1}^{n_c}Q_i(k)z(k-i), \qquad (5)$$

where the coefficient matrices $P_i(k)\in\mathbb{R}^{l_u\times l_u}$, $Q_i(k),R(k)\in\mathbb{R}^{l_u\times l_z}$ are updated by the RCAC algorithm.

We rewrite (5) as

$$u(k)=\Phi(k)\theta(k), \qquad (6)$$

where the regressor matrix $\Phi(k)$ is defined by

$$\Phi(k)\triangleq I_{l_u}\otimes\phi^{\mathrm T}(k)\in\mathbb{R}^{l_u\times l_\theta}, \qquad (7)$$

where

$$\phi(k)\triangleq[\hat\mu(k-1)^{\mathrm T}\ \cdots\ \hat\mu(k-n_c)^{\mathrm T}\ z(k-1)^{\mathrm T}\ \cdots\ z(k-n_c)^{\mathrm T}]^{\mathrm T},$$

$$\theta(k)\triangleq\mathrm{vec}\left[\ P_1(k)\cdots P_{n_c}(k)\ Q_1(k)\cdots Q_{n_c}(k)\ \right]\in\mathbb{R}^{l_\theta},$$

$l_\theta\triangleq l_u^2n_c+l_ul_yn_c$, "$\otimes$" is the Kronecker product, and "vec" is the column-stacking operator.

A. Retrospective Performance Variable

We define the retrospective performance variable

$$\hat z(k)=z(k)+G_f(\mathbf q)(\Phi(k)\hat\theta-u(k)), \qquad (8)$$

where $\mathbf q$ is the forward-shift operator, $\hat\theta\in\mathbb{R}^{l_\theta}$ contains the controller coefficients to be optimized,

$$G_f(\mathbf q)=\sum_{i=1}^{n_f}N_i\mathbf q^{-i}, \qquad (9)$$

and, for all $i=1,\ldots,n_f$, $N_i\in\mathbb{R}^{l_y\times l_u}$. G_f is an FIR filter of order n_f whose choice is discussed below. We rewrite (8) as

$$\hat z(k)=z(k)+N\Phi_b(k)\hat\theta-NU_b(k), \qquad (10)$$

where

$$N\triangleq\left[\ N_1\ \ \cdots\ \ N_{n_f}\ \right]\in\mathbb{R}^{l_y\times n_fl_u},$$

$$\Phi_b(k)\triangleq\begin{bmatrix}\Phi(k-1)\\ \vdots\\ \Phi(k-n_f)\end{bmatrix}\in\mathbb{R}^{l_un_f\times l_\theta},$$

$$U_b(k)\triangleq\begin{bmatrix}u(k-1)\\ \vdots\\ u(k-n_f)\end{bmatrix}\in\mathbb{R}^{l_un_f}.$$

The vector $\hat\theta$, which contains the controller coefficients, is determined by minimizing the retrospective cost function, as described next.

B. Retrospective Cost Function

Using the retrospective performance variable $\hat z(k)$, we define the retrospective cost function

$$J(k,\hat\theta)\triangleq\sum_{i=1}^{k-1}\lambda^{k-i}\big(\hat z(i)^{\mathrm T}R_z\hat z(i)+\hat\theta^{\mathrm T}\Phi_b(i)^{\mathrm T}N^{\mathrm T}R_fN\Phi(i)_b\hat\theta+\\ \hat\theta^{\mathrm T}\Phi(i)^{\mathrm T}R_u\Phi(i)\hat\theta\big)+\lambda^k\hat\theta^{\mathrm T}R_\theta\hat\theta, \qquad (11)$$

where R_z,R_f,R_u, and R_θ are positive-definite matrices, and $\lambda\le1$ is the forgetting factor. The following result uses recursive least squares (RLS) to minimize (11).

Proposition III.1. Let $P(0)=R_\theta^{-1}$ and $\theta(0)=0$. Then, for all $k\ge1$, the retrospective cost function (11) has a unique global minimizer $\theta(k)$, which is given by

$$\theta(k)=\theta(k-1)-P(k)\begin{bmatrix}N\Phi_b(k-1)\\ \Phi(k-1)\end{bmatrix}^{\mathrm T}\begin{bmatrix}R_z&0\\0&R_u\end{bmatrix}\\ \cdot\begin{bmatrix}N\Phi_b(k-1)\theta(k-1)+z(k-1)-NU_b(k-1)\\ \Phi(k-1)\theta(k-1)\end{bmatrix}, \qquad (12)$$

$$P(k)=\lambda^{-1}P(k-1)-\lambda^{-1}P(k-1)\begin{bmatrix}N\Phi_b(k-1)\\ \Phi(k-1)\end{bmatrix}^{\mathrm T}\\ \cdot\Gamma(k)^{-1}\begin{bmatrix}N\Phi_b(k-1)\\ \Phi(k-1)\end{bmatrix}P(k-1), \qquad (13)$$

where

$$\Gamma(k)\triangleq\lambda\begin{bmatrix}R_z&0\\0&R_u\end{bmatrix}^{-1}+\begin{bmatrix}N\Phi_b(k-1)\\ \Phi(k-1)\end{bmatrix}P(k-1)\\ \cdot\begin{bmatrix}N\Phi_b(k-1)\\ \Phi(k-1)\end{bmatrix}^{\mathrm T}. \qquad (14)$$

Furthermore, the control input at step k is given by

$$u(k)=\Phi(k)\theta(k). \qquad (15)$$

C. The Target Model G_f

The following result shows that the control $u(k)$ is constrained to the subspace spanned by the transposes of the coefficients of G_f.

Theorem III.1. Let $R_\theta=\beta I_{l_\theta}$, $R_u=\gamma I_{l_u}$ and let $\theta(k)$ be given by (15). Let $\Phi\triangleq I_{l_u}\otimes\phi^{\mathrm T}$, where $\phi\in\mathbb{R}^{l_\phi}$, and $l_\phi\triangleq l_\theta/l_u$. Then, for all $k\ge1$,

$$\Phi\theta(k)\in\mathcal{R}\left(\left[\ N_1^{\mathrm T}\ \ \cdots\ \ N_{n_f}^{\mathrm T}\ \right]\right). \qquad (16)$$

The following proposition follows from Theorem III.1.

Proposition III.2. Let $R_\theta = \beta I_{l_\theta}$, $R_u = \gamma I_{l_u}$ and let $\theta(k)$ be given by (15). Then, for all $k \geq 1$,

$$u(k) = \Phi(k)\theta(k) \in \mathcal{R}\left(\left[\begin{array}{ccc} N_1^{\mathrm{T}} & \cdots & N_{n_{\mathrm{f}}}^{\mathrm{T}} \end{array}\right]\right). \tag{17}$$

IV. Illustrative Examples

In this section, we present several examples demonstrating control allocation based on RCAC.

A. Colocated actuators

Consider the two-input, one-output discrete-time system

$$x(k+1) = Ax(k) + Bu(k), \tag{18}$$

$$y(k) = Cx(k), \tag{19}$$

where

$$A = \left[\begin{array}{cccc} -0.2650 & -0.2225 & -0.0938 & -0.1211 \\ -0.0727 & 0.3296 & 0.0594 & -0.3238 \\ 0.2661 & -0.2316 & 0.1396 & 0.2074 \\ -0.2016 & -0.1591 & 0.8285 & 0.1352 \end{array}\right], \tag{20}$$

$$B = \left[\begin{array}{cc} 0.8752 & 0.8752 \\ 0.3179 & 0.3179 \\ 0.2732 & 0.2732 \\ 0.6765 & 0.6765 \end{array}\right], \tag{21}$$

$$C = \left[\begin{array}{cccc} 0.8700 & 0.2437 & 0.8429 & 0.5577 \end{array}\right]. \tag{22}$$

The identical columns of B indicate that the two actuators are colocated. Let the command r be a unit step. We set

$$G_{\mathrm{f}}(\mathbf{q}) = N_1\mathbf{q}^{-1} = \left[\begin{array}{cc} 0.5 & 1 \end{array}\right]\mathbf{q}^{-1}, \tag{23}$$

$n_{\mathrm{c}} = 2$, and $R_\theta = 10^{-3} I_{l_\theta}$. With this choice of G_{f}, the control input $u(k)$ produced by RCAC is such that $u_2(k) = 2u_1(k)$ for all k. Figure 2 shows the closed-loop response of the system.

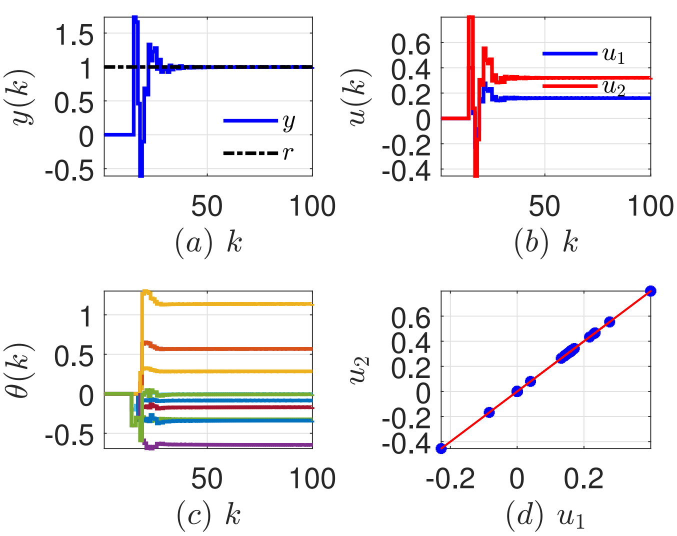

Fig. 2: Example IV-A. Control allocation for setpoint command following. (a) shows the response y, (b) shows the control signal u generated by RCAC, (c) shows the controller coefficients θ adapted by RCAC, and (d) shows the control signals. In (d), the direction of N_1^{T} is shown in red.

B. Independent actuators

We reconsider the plant in Example IV-A with the modified input matrix

$$B = \left[\begin{array}{cc} 0.8752 & 0.0712 \\ 0.3179 & 0.1966 \\ 0.2732 & 0.5291 \\ 0.6765 & 0.1718 \end{array}\right]. \tag{24}$$

Let the command r be a unit step. We set

$$G_{\mathrm{f}}(\mathbf{q}) = N_1\mathbf{q}^{-1} = \left[\begin{array}{cc} 0.5 & 1 \end{array}\right]\mathbf{q}^{-1}, \tag{25}$$

$n_{\mathrm{c}} = 2$, and $R_\theta = 10^{-3} I_{l_\theta}$. With this choice of G_{f}, the control input produced by RCAC is in the direction N_1^{T}. Figure 3 shows the closed-loop response of the system.

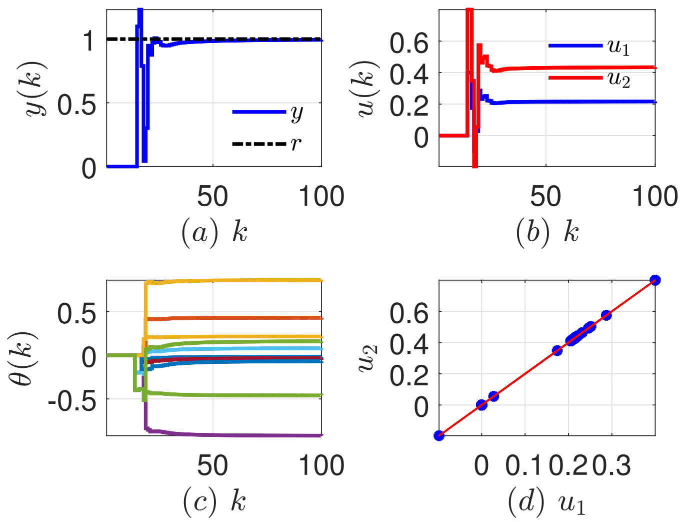

Fig. 3: Example IV-A. Control allocation for setpoint command following. (a) shows the response y, (b) shows the control signal u generated by RCAC, (c) shows the controller coefficients θ adapted by RCAC, and (d) shows the control signals. In (d), the direction of N_1^{T} is shown in red.

C. Uncontrollable channels

We reconsider the plant in Example IV-A with the modified input matrix

$$B = \left[\begin{array}{cc} b_1 & b_2 \end{array}\right] = \left[\begin{array}{cc} 0.8826 & 0.0984 \\ 0.5405 & 0.2135 \\ 0.0808 & 0.5128 \\ 0.3543 & 0.2059 \end{array}\right]. \tag{26}$$

Note that (A, b_1) and (A, b_2) each have one uncontrollable mode, but (A, B) is controllable. Hence, u_1 and u_2 must work together to achieve the control objective. Let the command r be a unit step. We set

$$G_{\mathrm{f}}(\mathbf{q}) = N_1\mathbf{q}^{-1} = \left[\begin{array}{cc} 0.5 & 1 \end{array}\right]\mathbf{q}^{-1}, \tag{27}$$

$n_{\mathrm{c}} = 2$, and $R_\theta = 10^{-3} I_{l_\theta}$. With this choice of G_{f}, the control input produced by RCAC is in the direction N_1^{T}. Figure 4 shows the closed-loop response of the system.

V. Lateral Control Allocation for an Aircraft

We now apply RCAC to the NASA generic transport model (GTM) [8]–[11], where the goal is to demonstrate control allocation for lateral motion. The GTM model includes an aerodynamic data base, trim function, and interface to facilitate feedback control from realistic sensors to thrust and control surfaces.

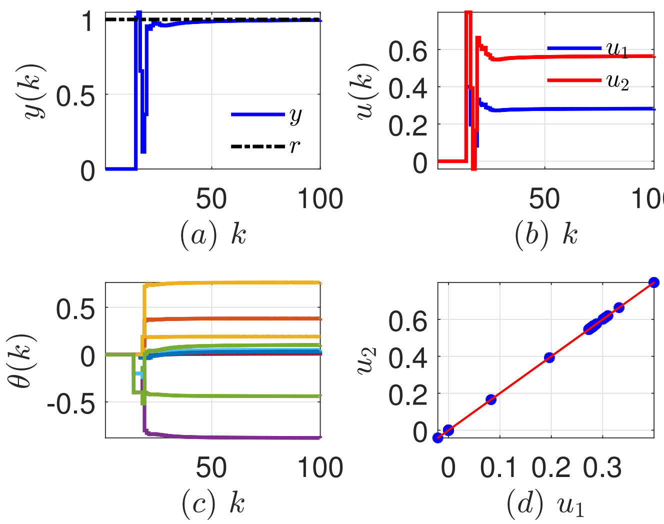

Fig. 4: Example IV-A. Control allocation for setpoint command following. (a) shows the response y, (b) shows the control signal u generated by RCAC, (c) shows the controller coefficients θ adapted by RCAC, and (d) shows the control signals. In (d), the direction of $N_1^{\rm T}$ is shown in red.

A. Control Architecture

Let $V_{\rm AC}$, h, τ, β, γ denote the airspeed, altitude, turn rate, sideslip angle, and flight-path angle, respectively. The aircraft lateral control inputs are $\boldsymbol{a}$ and $\boldsymbol{r}$, which denote ailerons and rudder, respectively. We define the measurement increment $\delta\tau(k) \triangleq \tau(k) - \tau_{\rm trim}$, where the subscript "trim" refers to the initial trim flight, and k denotes the current time step. We choose the sample time to be 0.1 sec. The performance variable z is given by the error signal

$$z(k) \triangleq \tau(k) - \tau_{\rm cmd}(k) = \delta\tau(k) - \delta\tau_{\rm cmd}(k), \tag{28}$$

where $\tau_{\rm cmd}$ is the turn-rate command, and $\delta\tau_{\rm cmd} \triangleq \tau_{\rm AC,cmd} - \tau_{\rm AC,trim}$ is the incremental turn-rate command. Let the requested actuator settings be denoted by

$$\boldsymbol{a}_{\rm req}(k) \triangleq \boldsymbol{a}_{\rm trim} + \delta\boldsymbol{a}_{\rm req}(k), \tag{29}$$

$$\boldsymbol{r}_{\rm req}(k) \triangleq \boldsymbol{r}_{\rm trim} + \delta\boldsymbol{r}_{\rm req}(k), \tag{30}$$

where the first term on the right-hand side is the constant actuator setting for the initial trim, and the second term on the right-hand side is the requested actuator setting increment specified by RCAC. Due to the actuator dynamics, the requested actuator settings may not be equal to the actual actuator settings, which are denoted by

$$\boldsymbol{a}_{\rm actual}(k) \triangleq \boldsymbol{a}_{\rm trim} + \delta\boldsymbol{a}_{\rm actual}(k), \tag{31}$$

$$\boldsymbol{r}_{\rm actual}(k) \triangleq \boldsymbol{r}_{\rm trim} + \delta\boldsymbol{r}_{\rm actual}(k), \tag{32}$$

where the left-hand side is the actual actuator setting, and the second term on the right-hand side is the actual actuator setting increment.

For lateral control, RCAC updates a strictly proper dynamic controller represented in input-output form as

$$\begin{bmatrix}\delta\boldsymbol{a}_{\rm req}(k) & \delta\boldsymbol{r}_{\rm req}(k)\end{bmatrix}^{\rm T} = \Phi(k)\theta(k), \tag{33}$$

where $\Phi(k) \triangleq I_{l_u} \otimes \phi^{\rm T}(k) \in \mathbb{R}^{l_u \times l_\theta}$, and

$$\phi(k) \triangleq \begin{bmatrix} \begin{bmatrix}\delta\boldsymbol{a}_{\rm actual}(k-1) & \delta\boldsymbol{r}_{\rm actual}(k-1)\end{bmatrix}^{\rm T} \\ \vdots \\ \begin{bmatrix}\delta\boldsymbol{a}_{\rm actual}(k-n_{\rm c}) & \delta\boldsymbol{r}_{\rm actual}(k-n_{\rm c})\end{bmatrix}^{\rm T} \\ \begin{bmatrix}\delta\tau_{\rm cmd}(k-1) & \cdots & \delta\tau_{\rm cmd}(k-n_{\rm c})\end{bmatrix}^{\rm T} \\ \begin{bmatrix}z(k-1) & \cdots & z(k-n_{\rm c})\end{bmatrix}^{\rm T} \\ \begin{bmatrix}\delta\beta(k-1) & \cdots & \delta\beta(k-n_{\rm c})\end{bmatrix}^{\rm T} \end{bmatrix}. \tag{34}$$

As shown in Figure 5, lateral control of GTM uses ailerons and rudder to follow the turn-rate command. In doing so, RCAC uses the turn-rate command as a feedforward signal, turn-rate command-following error as a feedback signal, and sideslip angle as a coupling feedback signal.

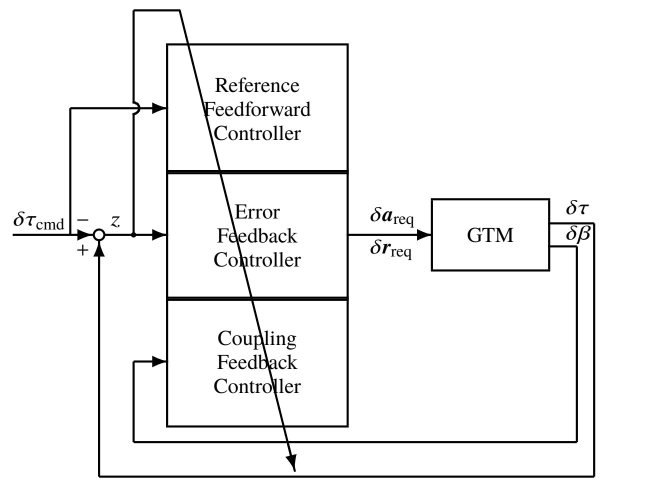

Fig. 5: Block diagram for lateral control of the NASA GTM model using aileron and rudder to follow turn-rate commands. The error signal z for the control is the difference $\delta\tau - \delta\tau_{\rm cmd}$. The controller also uses sideslip angle increment for feedback.

B. Simulation Setup

At the start of each example, the aircraft is assumed to be flying in an initial trim without the use of feedback control. The components of the controller coefficient vector θ are thus initially set to zero, that is, $\theta(0) = 0$. RCAC must therefore adapt the components of θ from their initial zero values to suitable nonzero values. As in [12], [13], in order to assist in the transition from open-loop to closed-loop control, we introduce zero-mean white noise with standard deviation 0.001 deg into ailerons and rudder from $t = 10$ sec to $t = 70$ sec. Let $a < 0$, $b < 0$, and define $N_4 \triangleq [a\ b] \in \mathbb{R}^{1\times 2}$. We set

$$G_{\rm f}(\mathbf{q}) = N_4\mathbf{q}^{-4}, \tag{35}$$

$n_{\rm c} = 8$, $R_\theta = 10^{-2} I_{l_\theta}$, and

$$R_u(k) = \begin{cases} 10 I_2, & z^2(k) > 1, \\ 10.1(z^2(k) - 0.01) I_2, & 0.109 \le z^2(k) \le 1, \\ I_2, & z^2(k) < 0.109. \end{cases} \tag{36}$$

Note that R_u increases linearly as a function of z^2 within the interval $[0.01, 1]$. Furthermore, note that, by choosing a

and b, the ratio of the usage of ailerons and rudder can be specified.

For all the following examples, GTM is initialized with the trim

$$
\begin{aligned}
V_{\mathrm{AC}}(0) = V_{\mathrm{AC,trim}} = 100.6 \text{ kt}, \ \gamma(0) = \gamma_{\mathrm{trim}} = 0 \ \text{deg}, \\
\tau(0) = \tau_{\mathrm{trim}} = 0 \ \text{deg/sec}, \ \beta(0) = \beta_{\mathrm{trim}} = 0 \ \text{deg}, \\
\alpha(0) = \alpha_{\mathrm{trim}} = 3 \ \text{deg}, \ h(0) = 8000 \text{ ft}.
\end{aligned} \tag{37}
$$

The incremental turn-rate command is given by

$$
\delta\tau_{\mathrm{cmd}}(k) = \begin{cases} 0, & k < 1000, \\ \min\{5, 0.005(k-1000)\}\,\text{deg/sec}. & k \geq 1000, \end{cases} \tag{38}
$$

In addition to the turn-rate command, the aircraft is commanded to hold the airspeed and altitude. Note that the command is to trim the aircraft in horizontal circular flight with turn-rate 5 deg/sec from the initial straight-line trim flight (37).

C. Horizontal Circular Flight With Equalized Control Allocation

We set $a = -1$ and $b = -1$, and thus the control allocation is equalized between the ailerons and rudder channels. Figure 6 shows that, after the initial adaptation, the maximum command-following error for turn-rate is 0.35 deg/sec. At $t = 300$ sec, the command-following error for turn-rate is 0.06 deg/sec. Figures 7(a) and 7(b) show the RCAC generated ailerons and rudder settings, respectively. Note that the transients from $t = 10$ sec to $t = 70$ sec is due to the actuator noise warmup. Figure 8(a) shows θ converges after the initial adaptation, and subsequently brings the aircraft back to its initial trim at $t = 80$ sec. Figure 8(b) shows the requested and actual control signals. Note that the control is constrained in the direction N_4^{T}.

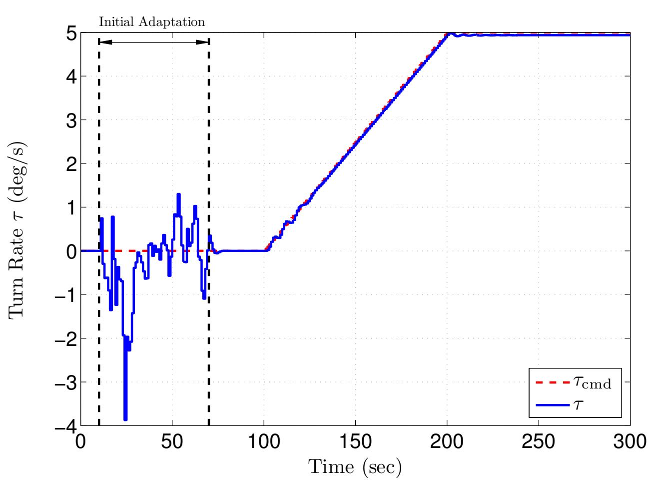

Fig. 6: Horizontal circular flight with equalized lateral control allocation. After the initial adaptation, the maximum command-following error for turn-rate is 0.35 deg/sec. At $t = 300$ sec, the command-following error for turn rate is 0.06 deg/sec.

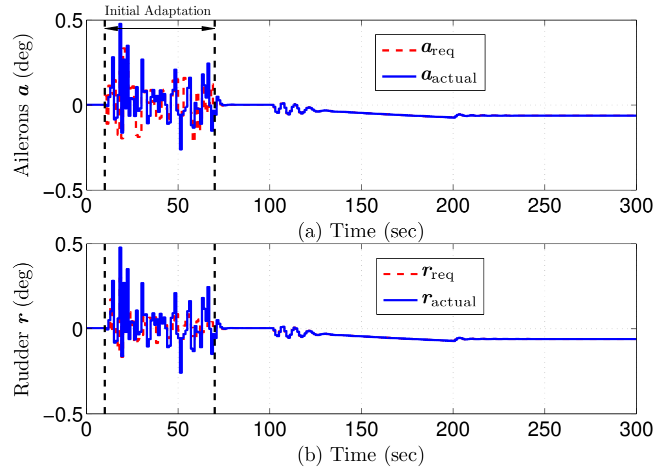

Fig. 7: Horizontal circular flight with equalized lateral control allocation. (a) Requested and actual ailerons settings. (b) Requested and actual rudder settings.

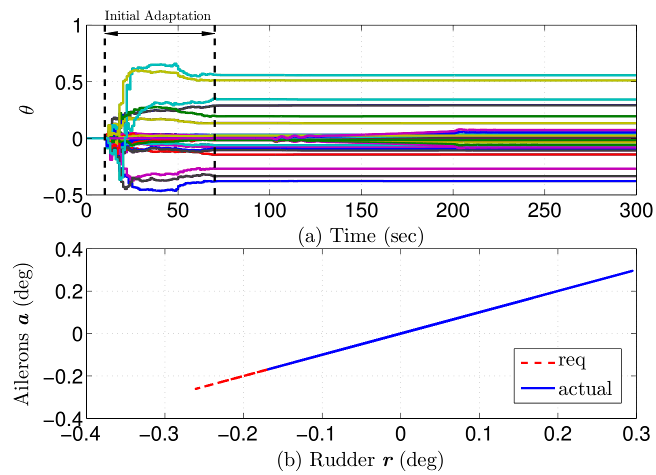

Fig. 8: Horizontal circular flight with equalized lateral control allocation. (a) θ converges after the initial adaptation, and subsequently brings the aircraft back to its initial trim at $t = 80$ sec. (b) The requested and actual control signals are constrained in the direction N_4^{T}.

D. Horizontal Circular Flight With Unequalized Control Allocation

We now set $a = -2$ and $b = -1$, and thus the control allocation is unequalized among the ailerons and rudder channels. Figure 9 shows that, after the initial adaptation, the maximum command-following error for turn-rate is 0.16 deg/sec. At $t = 300$ sec, the command-following error for turn rate is 0.04 deg/sec. Figures 10(a) and 10(b) show the RCAC generated ailerons and rudder settings, respectively. Note that the transients from $t = 10$ sec to $t = 70$ sec is due to the actuator noise warmup. Figure 11(a) shows θ converges after the initial adaptation, and subsequently brings the aircraft back to its initial trim at $t = 80$ sec. Figure 11(b) shows the requested and actual control signals. Note that the control is constrained in the direction N_4^{T}.

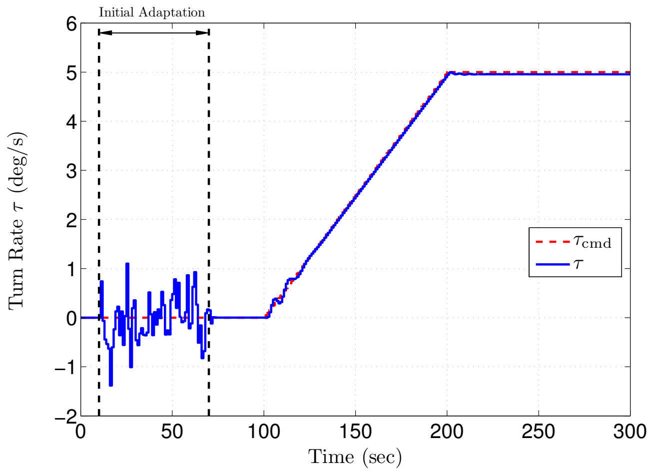

Fig. 9: Horizontal circular flight with unequalized lateral control allocation. After the initial adaptation, the maximum command-following error for turn-rate is 0.16 deg/sec. At $t = 300$ sec, the command-following error for turn-rate is 0.04 deg/sec.

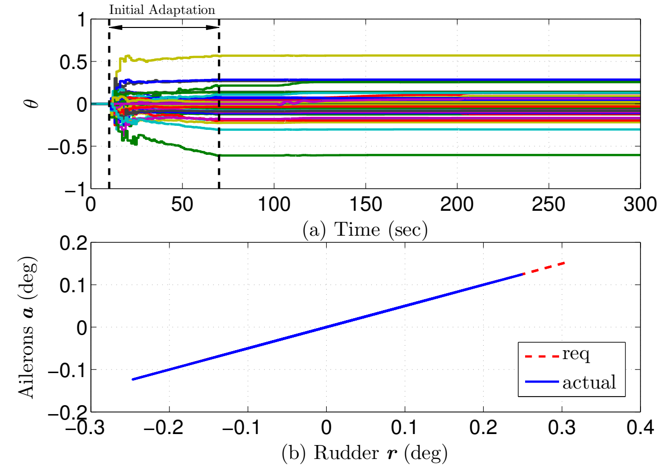

Fig. 11: Horizontal circular flight with unequalized lateral control allocation. (a) θ converges after the initial adaptation, and subsequently brings the aircraft back to its initial trim at $t = 80$ sec. (b) The requested and actual control signals are constrained in the direction N_4^{T}.

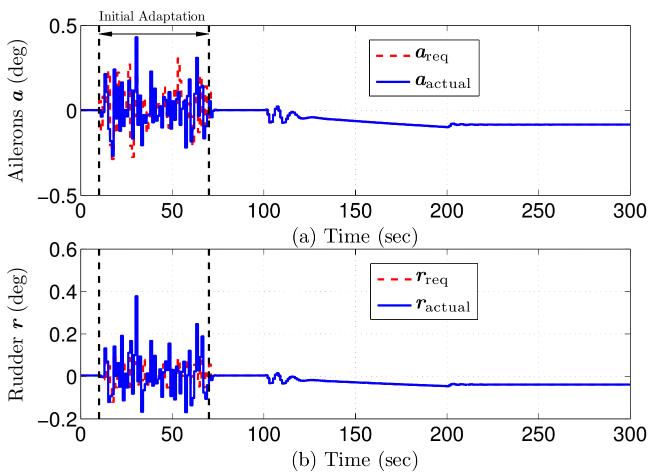

Fig. 10: Horizontal circular flight with unequalized lateral control allocation. (a) Requested and actual ailerons settings. (b) Requested and actual rudder settings.

VI. Conclusions

This paper presented a novel approach to control allocation for wide systems within the context of retrospective cost adaptive control (RCAC). The approach is based on the fact that the control input is constrained to the range of the transpose of the target model. This technique was applied to illustrative examples as well as lateral control of the nonlinear NASA GTM model.

The illustrative examples that were considered are minimum phase, and thus it was not necessary to account for the presence of NMP zeros. Although NMP zeros are nongeneric in nonsquare plants, they arise generically in square systems (with SISO plants as the special case 1×1). It is thus of interest to consider control allocation for NMP square systems. The challenge is thus to enforce control allocation by choosing G_{f} to also account for the presence of NMP zeros.

References

[1] O. Härkegård and S. T. Glad, "Resolving actuator redundancy–optimal control vs. control allocation," *Automatica*, vol. 41, pp. 137–144, 2005.

[2] T. A. Johansen and T. I. Fossen, "Control allocationâĂŤA survey," *Automatica*, vol. 49, pp. 1087–1103, 2013.

[3] W. C. Durham, "Constrained Control Allocation," *AIAA J. Guid. Contr. Dyn.*, vol. 16, pp. 717–725, 1993.

[4] D. F. Enns, "Control Allocation Approaches," in *Proc. Guid. Nav. Contr. Conf.*, Boston, August 1998, AIAA-98-4109.

[5] J. J. Burken, P. Lu, Z. Wu, and C. Bahm, "Two Reconfigurable Flight-Control Design Methods: Robust Servomechanism and Control Allocation," *AIAA J. Guid. Contr. Dyn.*, vol. 24, pp. 482–493, 2001.

[6] M. Bodson, "Evaluation of Optimization Methods for Control Allocation," *AIAA J. Guid. Contr. Dyn.*, vol. 25, pp. 703–711, 2002.

[7] Y. Rahman, A. Xie, and D. S. Bernstein, "Retrospective Cost Adaptive Control: Pole Placement, Frequency Response, and Connections with LQG Control," *IEEE Contr. Sys. Mag.*, vol. 37, pp. 28–69, October 2017.

[8] T. Jordan, W. Langford, C. Belcastro, J. Foster, G. Shah, G. Howland, and R. Kidd, "Development of a Dynamically Scaled Generic Transport Model Testbed for Flight Research Experiments," *AUVSI Unmanned Unlimited, Arlington, VA*, 2004.

[9] R. M. Bailey, R. W. Hostetler, K. N. Barnes, C. M. Belcastro, and C. M. Belcastro, "Experimental Validation: Subscale Aircraft Ground Facilities and Integrated Test Capability," in *Proc. AIAA Guid. Nav. Cont. Conf.*, San Francisco, CA, 2005, AIAA-2005-6433.

[10] T. L. Jordan and R. M. Bailey, "NASA Langley's AirSTAR Testbed: A Subscale Flight Test Capability for Flight Dynamics and Control System Experiments," in *Proc. AIAA Guid. Nav. Cont. Conf.*, Honolulu, HI, 2008, pp. 18–21, AIAA-2008-6660.

[11] K. Cunningham, D. E. Cox, D. G. Murri, and S. E. Riddick, "A Piloted Evaluation of Damage Accommodating Flight Control Using a Remotely Piloted Vehicle," in *Proc. AIAA Guid. Nav. Cont. Conf.*, Portland, OR, 2011, AIAA-2011-6451.

[12] A. Ansari and D. S. Bernstein, "Retrospective Cost Adaptive Control of the Generic Transport Model Under Uncertainty and Failure," *J. Aerospace Information Systems*, vol. 14, no. 3, pp. 123–174, 2017.

[13] A. Ansari and D. Bernstein, "Retrospective Cost Adaptive Control of the Generic Transport Model under Abrupt Faults," in *2018 AIAA Guidance, Navigation, and Control Conference*, 2018, p. 1125.